Revision 1

Transition metal cation site preferences in forsterite (Mg_2SiO_4) determined from paramagnetically shifted NMR resonances.

Ryan J. McCarty[1]*, Aaron C. Palke[1] **, Jonathan F. Stebbins[1], J. Stephen Hartman[2]

[1]Department of Geological and Environmental Sciences, Stanford University, Stanford, CA 94305, USA

[2]Department of Chemistry, Brock University, St. Catharines, Ontario L2S 3Al Canada

*corresponding author, ryanjm@stanford.edu

**current address: Gemological Institute of America, Carlsbad, CA 92008, USA

Abstract

In marked contrast to the single, narrow ^{29}Si MAS NMR resonance for pure forsterite (Mg_2SiO_4), the spectra for synthetic forsterite containing 0.05 to 5 % of the Mg^{2+} replaced with Ni^{2+}, Co^{2+}, or Fe^{2+} display between 4 and 26 additional, small, paramagnetically shifted peaks that are caused by interactions of the unpaired electron spins on the transition metal cations and the nuclear spins. Analyses of these relative peak areas, their numbers, and comparison of their positions to those in spectra of synthetic monticellites ($CaMgSiO_4$) containing similar levels of transition metals, allows at least partial assignment to the effects of cations in either the M1 octahedral site only, or to both M1 and M2 sites. More detailed analyses indicate that in forsterite, Ni^{2+} occupies only M1, Fe^{2+} occupies M1 and M2 roughly equally, and Co^{2+} occupies both M1 and M2 in an approximately 3:1 ratio. These findings for low concentrations agree

with expectations from previous studies by other methods (e.g. XRD) of olivines with much higher transition metal cation contents. However, even low concentrations of Mn^{2+} (e.g. 0.1%), as well as higher Fe^{2+} contents (e.g. in natural San Carlos olivine) can broaden NMR peaks sufficiently to greatly reduce this kind of information content in spectra.

Keywords: Forsterite, olivine, NMR, transition metal cations, paramagnetic shift, site preference.

Introduction

Forsterite (Mg_2SiO_4) is the magnesium end member of olivine, a common mineral found in basaltic rocks and a major constituent of the earth's upper mantle (Harris et al. 1967). Significant research efforts have been invested in better understanding transition metal cation incorporation in forsterite, which can potentially refine partition coefficients used in numerous geothermometric and geobarometeric methods (Canil 1994; Loucks 1996; Wu and Zhao 2007). The structure of forsterite is well defined in the space group Pbnm, consisting of isolated silica tetrahedra connected by a network of octahedral Mg sites, M1 and M2. The latter provide two unique substitution environments for compatible, divalent transition metal cations, with the M1 site being smaller and more distorted than the M2 site (Brown 1980).

Multiple studies have converged on similar results for the site occupancies of divalent transition metal cations at high concentrations in olivines, providing a foundation for investigation of concentrations that approach minor to trace element levels. The review chapter by Brown (1980) provides a comprehensive summary of the early efforts on this problem. X-ray diffraction has been a primary tool when concentrations are high enough to

measurably affect the long-range crystal structure, such as the finding of the strong Ni^{2+} preference for the M1 site (Rajamani et al. 1975). Similarly, Co^{2+} has also been found to prefer the M1 site, though to a lesser degree than the Ni^{2+} preference (Ghose and Wan 1974). Varying results from different methods place bounds on the distribution of Fe^{2+}, which is usually found to occupy the two sites almost equally (Brown 1980). These distributions are largely determined by the greater crystal field stabilization energy for the M1 site, although the M2 site is increasingly favored as ionic radii increase (Brown 1980).

Further spectroscopic studies have confirmed and characterized these distributions. An EXAFS study of Ni-bearing forsterite outlined the changes in distribution with temperature and found an M1 site preference as well as a suggestion of clustering of Ni^{2+} into adjacent M1 sites (Henderson et al. 2001). The work of Taftø and Spence (1982) on natural San Carlos olivine samples (approximately 10% Fe_2SiO_4 component), using an electron-microscopic X-ray emission technique, determined that Fe^{2+} entered the two sites almost equally. A Mössbauer study on synthetic crystals with equal concentrations of Mg^{2+} and Fe^{2+} determined that at 500 ˚C, Fe slightly prefers the M1 site, a preference which increases as temperature rises to 800 ˚C (Morozov et al. 2006). The Rietveld refinement of Müller-Sommer et al. (1997) on synthetic Co-rich forsterite indicated a distribution of Co^{2+} between the two sites with an M1 site preference. Polarized optical absorption spectroscopy results additionally agree on the M1 preference of this cation (Taran and Rossman 2001). Confirmation of the M2 site preference of Mn^{2+} has been provided by channeling-enhanced X-ray emission spectroscopy (McCormick et al. 1987). The effects of temperature on transition metal site occupancies in olivines have been extensively studied by XRD and other methods for samples typically in the range of about 10 to 50 % of the

non-forsterite component, and have been analyzed thermodynamically, demonstrating systematically increasing M1 preference from Fe^{2+} to Co^{2+} to Ni^{2+} (Kroll et al. 2006; Morozov et al. 2006; Heinemann et al. 2007). The behavior of transition metal cations in forsterite at minor to trace element concentrations (below detection limits of many methods) is less well characterized, although as a first approximation they are predicted to behave similarly as at higher concentrations. In this paper we describe a novel application of Nuclear Magnetic Resonance (NMR) to this problem.

NMR is an element-specific spectroscopic method highly sensitive to coordination, bond length and ordering in solids, and is best known in structural studies of major elements in materials that are essentially free of ions with unpaired electron spins (Stebbins and Xue 2014). In many materials with high concentrations of transition metal or rare earth element cations, the intense local magnetic fields of the associated unpaired electrons can cause problematic NMR peak broadening and loss of structural information, although useful spectra have been recently obtained in systems such as cations sorbed on iron oxyhydroxides (Nielsen et al. 2005) and even for Mn and Fe phosphate battery materials (Grey and Dupré 2004). Early ^{29}Si MAS NMR studies noted severe peak broadening for synthetic olivines with 1 to 5 % Fe_2SiO_4 component, and even "no signal" for a natural olivine with 9% Fe_2SiO_4 (Grimmer et al. 1983). In a unique and detailed study of spin-lattice relaxation of sol-gel forsterites containing about 0.2 to 9% Ni, Co, and Cu, the effects of heterogeneity on non-exponential relaxation were documented, as well as significant peak broadening at higher Co contents (Hartman et al. 2007).

Recently, it has been found that in some silicate and phosphate minerals containing up to several % of such paramagnetic cations, well-resolved extra NMR peaks can be detected that are often shifted far outside the range of normal, diamagnetic "chemical" shifts (Bégaudeau et al. 2012; Stebbins and Xue 2014). These extra peaks are "paramagnetically shifted" (i.e. NMR frequency shifts that can be either positive or negative, caused by unpaired electrons of paramagnetic cations) and are due to either through-space dipolar couplings from an asymmetric cation site ("pseudo-contact shift") and/or to through-bond transfer of unpaired electron spin density to the observed nuclide ("Fermi contact shift") (Grey et al. 1989, 1990). These effects are highly sensitive to interatomic distances and to electron distributions, and hence on structural details such as bond distances and angles (Lee et al. 1998; Middlemiss et al. 2013), and have been clearly detected in first and in some cases second cation shells, i.e. up to four bonds away from an observed NMR nuclide such as ^{29}Si, ^{31}P, or ^{27}Al in phases such as zircon, garnets, pyroxenes, $MgSiO_3$ perovskites, and monazites/xenotimes (Bégaudeau et al. 2009, 2012; Stebbins and Kelsey 2009; Palke and Stebbins 2011a, 2011b; Palke et al. 2012, 2013,in press). Although it remains difficult to predict the magnitude and even the sign of paramagnetic frequency shifts from a hypothesized structure (e.g. a distribution of paramagnetic cations), geometric relations, relative frequency shifts, and observed peak areas can provide useful clues as to at least partial assignment of such peaks to given structural configurations. Such frequency shifts depend strongly on temperature (Bertini et al. 2002; Palke and Stebbins 2011a; Palke and Stebbins 2011b), providing a convenient method to distinguish them from ordinary chemical shifts.

Paramagnetic shifts were first described in olivine through observation of numerous unexpected, small, "extra" resonances in an unusually high-quality ^{29}Si NMR spectrum of isotopically-enriched forsterite bearing about 0.1% Co^{2+} (Stebbins et al. 2009b). In this paper, we describe a systematic study of paramagnetically shifted peaks in ^{29}Si MAS NMR spectra of forsterite with 0.05 to 5 cation % Ni^{2+}, Co^{2+}, Fe^{2+}, and Mn^{2+}, following up on preliminary studies (McCarty et al. 2012, 2014). Such spectra can be quite complex, with more than two dozen resolvable resonances caused by a single paramagnetic species, in marked contrast to the single resonance of pure Mg_2SiO_4. We use the symmetry elements in the crystal structure, coupled with probabilistic predictions, to limit the possible configurations of transition metal cations relative to Si, and produce quantitative and bounded descriptions of the site occupancies. We also investigate synthetic monticellite ($CaMgSiO_4$) bearing the same cations, as their expected lack of M2 site occupancy helps to identify M1 features in the corresponding forsterite spectra, increasing the confidence of the derived site distributions. Observed relative peak areas ultimately correspond to transition metal cation site distributions, which are reported for Ni, Fe and Co. We also show the limits of this method in olivine, as some minor cations in even low concentrations (e.g. Mn^{2+}), and geologically interesting concentrations of more common constituents (e.g. Fe^{2+} in San Carlos olivine) can cause severe NMR peak broadening.

Experimental Methods

Samples

We initially studied a series of forsterite samples synthesized by a sol-gel/low temperature sintering process, containing up to about 5% Co, Mn, or Ni, which were the subject of a previous report on the effects of heterogeneous paramagnetic cation distributions on spin-lattice relaxation (Hartman et al. 2007). We attempted to increase the homogeneity of these samples by sintering at 1500 ˚C for 2 to 4 days with intermediate grinding and pellet pressing steps. However, grain growth was slow under these conditions, resulting in loose aggregates of mostly sub-micron particles with a few larger crystals. EPMA data (see below) showed no areas with high transition metal concentrations, but did suggest considerable heterogeneity as well as up to about 10% excess MgO, suggesting the presence of this "impurity" phase which may have somehow inhibited recrystallization. Preliminary ^{29}Si MAS NMR on these samples identified relatively high contents of enstatite in many, further suggesting heterogeneity, but were useful in indicating the ranges of concentration where each transition metal would yield relatively well-resolved spectra. The difficulty in homogenizing these materials led us to synthesize a new group of forsterites from high temperature sintered oxide powders. All data shown here are from this latter group.

Reagent grade SiO_2 (dehydrated silica gel), MgO, $CaCO_3$, NiO, FeO, Co_3O_4, $MnCO_3$ and CuO were used for the high temperature powder syntheses. For forsterite, an excess of approximately 1 wt% MgO was added to otherwise on-composition mixtures to reduce the chance of formation of unwanted silicates such as pyroxene. Monticellite was produced from stoichiometric mixtures. Samples are labeled by the mole percent of the added transition metal cation (M) that replaces Mg in forsterite ($Mg_{2-2x}M_{2x}SiO_4$) or Mg+Ca in monticellite ($CaMg_{1-2x}M_{2x}SiO_4$), as determined by electron microprobe analyses (Table 1). For instance, a Fe-

148 monticellite sample with the formula $CaMg_{0.998}Fe_{0.002}SiO_4$ is labeled "0.1% Fe-monticellite." This
149 notation allows an easy comparison between both forsterite and monticellite sample
150 concentrations and spectra. Compositions are also given in dopant atoms per formula unit
151 (apfu), i.e. 2x in the notation used here and 0.002 Fe atoms per $[Ca(Mg,Fe)SiO_4]$ unit in this
152 specific example.

153

154 Ni-, Co-, and Mn-forsterite were produced by grinding reagents together with isopropyl
155 alcohol in an agate mortar and then heating for 2 to 4 days in a platinum crucible at 1500 ˚C
156 with 2 to 4 intermediate grinding steps. After the initial heating, some samples were pressed
157 into pellets at 9 metric tons and heated again; however, pressed and un-pressed samples
158 showed no significant difference with respect to sample homogeneity. Unlike the sol-gel
159 forsterites, relatively rapid grain growth in sequential heat treatments was evident by the
160 formation of hard ceramic-like pellets and average grain sizes between 5 to 25 µm with some
161 crystals as large as 250 µm. Fe-forsterite was produced by buffering the oxygen pressure with
162 iron metal. For the 0.4% Fe sample, a drying step was added after grinding, and the sample was
163 heated to 1400 ˚C within a vacuum-sealed silica glass tube containing a piece of iron metal foil.
164 For the 0.05% Fe forsterite, a platinum-wrapped pellet of the starting material was heated to
165 1400 ˚C on a ceramic disk in a closed mild steel tube which self-sealed during heating in argon,
166 remaining unoxidized inside. Ni-, Co-, and Mn- cooling rates from 1500 ˚C to room temperature
167 range between 200 to 400 ˚C per hour. Fe- samples were quenched from 1400˚C to below 900

168 ˚C within 4 minutes. Samples bearing higher concentrations of Ni^{2+} displayed a light green hue,
169 lower concentration Co- and Fe-bearing samples appeared white.

170 Monticellite samples were synthesized by heating oxide mixtures between 1500 to 1600
171 ˚C for 4 to 6 hours followed by removal from the furnace and quenching in air to produce
172 crystal-glass mixtures. Samples were then ground with isopropyl alcohol in an agate mortar,
173 pressed into pellets at 9 metric tons and heated to 1300 ˚C for 2 to 4 days with 2 to 3
174 intermediate grinding steps. Low concentration Fe-monticellite was produced as described
175 above with an added heating to 1300 ˚C in a vacuum-sealed silica glass tube containing an iron
176 foil oxygen fugacity buffer.

177 In addition, we collected new spectra on a Co-bearing, 95% ^{29}Si-enriched forsterite
178 originally synthesized from oxide powders for studies of high pressure phases (Stebbins et al.
179 2009a, 2009b) and a sample of natural olivine from a mantle peridotite nodule (San Carlos, NM,
180 approximately $[Mg_{1.8}Fe_{0.2}]SiO_4$).

181 The samples grown by high temperature sintering of oxides were characterized in detail.
182 The JEOL JXA-8230 electron microprobe at Stanford University was used to determine sample
183 homogeneity and resulting sample compositions, using synthetic forsterite, wollastonite, metal
184 and oxide standards. NMR, EPMA and high-contrast backscattered electron images were used
185 to identify and characterize silicon-bearing impurity phases. All of these forsterite samples are
186 assumed to have a minor amount of periclase. Monticellite samples contain minor amounts of
187 one or more impurity phases, including akermanite, and possibly merwinite or forsterite. Some
188 samples were determined to have minor heterogeneities in transition metal concentrations,

but for the results shown here these are not significant, as minor compositional variations from grain to grain will not affect conclusions about overall site occupancies and we are not attempting to deduce details of localized transition metal ion clustering. Table 1 reports average compositions based on 8 to 18 EPMA points with one standard deviation indicated in parentheses. The higher temperature synthesis of the Ni^{2+} and Co^{2+} forsterites resulted in very homogeneous samples. The sample synthesis conditions of the Fe^{2+} samples made it difficult to consistently produce homogeneous samples. The NMR results of the least homogeneous sample (0.4% Fe-forsterite) are reported here only for comparison with the data for the lower concentration sample, although both spectra look similar. Despite the observation of additional phases, monticellite transition metal concentrations are close to homogenous, due in part to the initial high temperature heating step.

NMR

^{29}Si MAS NMR spectra were collected with a Varian Unity/Inova spectrometer at 14.1 Tesla (119.1 MHz) and a Varian Infinity Plus spectrometer at 9.4 Tesla (79.4 MHz), using Varian/Chemagnetics "T3" probes with 3.2 mm zirconia rotors. Simple one pulse acquisitions were used for almost all spectra with radiofrequency (RF) power levels of about 133 kHz and a typical RF tip angle of 30˚. For the San Carlos sample, the rapid signal decay necessitated the use of a spin-echo pulse sequence (90˚ - 180˚) with an echo delay of 100 μs, which may have excluded some of the broadest components of the spectrum. Spinning speeds of 9 to 20 kHz were used as shown in the figures; the slower speed reduced air frictional heating enough to

cause readily detectable changes in the positions of paramagnetically shifted peaks. From previous studies (Palke and Stebbins 2011b) we estimate that sample temperatures at 20 kHz spinning speed are about 40 to 50 ˚C, and close to room temperature at 9 kHz. On the 9.4 Tesla spectrometer a similar probe with 4 mm rotors and 9-15 kHz spinning speeds with variable temperature capabilities (25 to 150 ˚C) was also used. Paramagnetically shifted peaks were found to relax fully with short pulse delays of 0.05 s, which allowed high signal-to-noise spectra to be collected for these small features, each of which often had less than 0.8 % of the total NMR signal. Peak areas are reported relative to those obtained for the fully relaxed, unshifted central peaks, which required delay times of up to 3600 s to measure. Areas were obtained by fitting with mixed Gaussian/Lorentzian line shapes (Table 1), with spinning sideband areas included when observable.

Results

NMR spectra of the Ni-forsterite (Fig. 1), Fe-forsterite (Fig. 2), and Co-forsterite (Fig. 3) samples each display a major, unshifted peak at the expected position of -61.8 ±0.2 ppm for pure Mg_2SiO_4 forsterite, consistent with previous studies (Mägi et al. 1984), in addition to a number of small, paramagnetically shifted peaks, many of which are at frequencies above -60 ppm and thus outside of the known range of chemical shifts in silicates. The latter vary in number from approximately 4 in Ni-forsterite, 16 in Fe-forsterite and 26 in Co-forsterite, and all shift inward with the slightly higher temperature resulting from a faster spinning speed (Fig. 2), confirming their origin. In some instances comparison of spectra collected at 25 °C and 75 or

231 150 °C with the variable temperature probe was convenient to initially identify subtle
232 paramagnetically shifted features. Such peaks are related to SiO_4 tetrahedra with paramagnetic
233 Ni^{2+}, Fe^{2+}, or Co^{2+} in their first or second cation coordination shells, i.e. within 7 Å. In Figure 1,
234 the intensity of these peaks can be seen to increase with Ni^{2+} concentration while peak
235 positions remain unchanged. All paramagnetically shifted peaks are fully relaxed with a 0.05 s
236 pulse delay, although the main unshifted peaks are often only partially relaxed at this pulse
237 delay, especially for samples with lower dopant concentrations (Table 1). The widths of the
238 unshifted peaks tend to increase with increasing transition metal concentration, with a greater
239 Lorentzian component to the line shape (Table 1). A detailed study of the ^{29}Si spin-lattice
240 relaxation of Co-bearing forsterite, including the ^{29}Si-enriched sample described here, was
241 reported earlier (Stebbins et al. 2009a), documenting the effects of transition metal cation
242 concentration and the "stretched exponential" form of the relaxation curve.

243 Spectra for Ni^{2+}-, Co^{2+}-, and Fe^{2+}-bearing monticellite (Figs. 4, 5 and 6) contain the main,
244 unshifted monticellite peak at -65.5 ±0.5 ppm, as well as signals from low abundance impurity
245 phases akermanite (-73.7 ppm) and possibly merwinite or forsterite (-61.8 ppm). These spectra
246 contain fewer paramagnetically shifted peaks, which are closer to the primary monticellite peak
247 than the corresponding forsterite spectra. Visible paramagnetically shifted peaks are clearly
248 associated with the monticellite phase, not with these impurities, as they converge on the
249 unshifted monticellite peak positon with increasing temperature. No paramagnetically shifted
250 peaks could be obviously associated with the impurity phases. The unshifted akermanite peaks
251 relaxed somewhat more slowly than the main monticellite peaks, suggesting lower transition
252 metal contents in the former.

Paramagnetically shifted peaks are simply numbered from higher to lower frequencies, and positions and areas are given in Tables 2-7 for each sample. Hereafter, paramagnetically shifted peak positions are reported relative to those of the unshifted central resonances, i.e. the chemical shifts. In many cases, the main unshifted peak cannot be fit well with a single component and seems to contain low-intensity shoulders which likely are due to additional unresolved peaks with smaller paramagnetic shifts. The fitted intensities of these shoulders are reported; however, the significance of these values is unclear as their uncertainties are large. Reported peak area values are averages of spectra collected at two different magnetic fields and/or different spinning speeds; peak positions are reported from single spectra. The precision of peak area measurements are reported individually for each set of data. An overall accuracy of ±22% relative is estimated, resulting from the NMR experimental conditions and data processing.

Ni-containing samples

Figure 1 displays the ^{29}Si NMR spectra of three forsterites with Ni^{2+} concentrations of 0.25, 1 and 5 % (Table 2). The spectra each display four small paramagnetic shifted peaks with equal areas, labeled as 7, 9, 10 and 11. Peak 7 is shifted +20.8 ppm to higher frequency, peaks 9 and 10 are close together at +8.4 ppm and +5.8 ppm, respectively, and peak 11 is shifted down in frequency -6.4 ppm. The multiple peak positions indicate the various possible geometric relationships (bond paths, distances, etc.) of Ni^{2+} and Si and the equal area of these peaks is consistent with identical lattice sites.

For the highest concentration sample, 5% Ni-forsterite, the four peaks described above are joined by additional smaller paramagnetically shifted peaks numbered 1, 2, 3, 4, 5, 6 and 8 (peaks 5, 6 and 8 are also barely visible in the 1% Ni sample). As discussed in detail below, their positions and their appearance only at higher concentrations indicate that these low intensity features result from Si in sites with two or even three Ni^{2+} cation neighbors. A peak area detection limit of about 0.1 % is possible in the 5% sample, setting an upper bound on possible unresolvable peak areas.

In Figure 4 the spectrum of 1% Ni-monticellite (Table 3) presents 3 paramagnetically shifted peaks, peaks 1 and 2 at the higher frequencies of +14.2 ppm and +3.1 ppm respectively, and peak 3 at -3.1 ppm. Peaks 1 and 3 have comparable areas but 2 has slightly more than twice this area. When compared to the Ni-forsterite spectra, peak positions have the same relative locations with Ni-monticellite peak 2 apparently being the sum of overlapping peaks corresponding to Ni-forsterite peaks 9 and 10. A peak at the known chemical shift of akermanite at -73.6 ppm (Stebbins 1995) is present as well as a shoulder from an unidentified impurity phase at -72.4 ppm. In addition to the clearly identifiable paramagnetically shifted peaks, several low-intensity features near the limit of detection in this sample (>0.1%) are observed and are likely to be of similar origin. However, these less well-defined features are not important in the following discussion. NMR spectra of the Ni-bearing sol-gel forsterites showed many of the same paramagnetically shifted peaks, but are not shown here and were not analyzed in detail because of concerns about heterogeneity

Fe-containing samples

Figure 2 displays the ^{29}Si NMR spectra of 0.05% Fe-forsterite (Table 4) at two spinning speeds. 16 paramagnetically shifted peaks are observed. 9 peaks are shifted to higher frequencies and 7 to lower frequencies, many of which are overlapping. Peak areas vary somewhat. Peak 9 is difficult to resolve in the central transition, but is clearly distinguished in the spinning sidebands, where the contribution from the central, unshifted peak is often relatively much smaller (Fig. 7). Areas of peaks 6 through 11 are difficult to constrain due to significant overlap with the main, unshifted peak. Due to variations in sideband intensities for the paramagnetically shifted peaks, it was necessary to carefully fit the sideband manifolds and include these in the reported intensities. For example, peak 14 in the 12 kHz spectrum is noticeably smaller than in the 20 kHz spectrum, a result of the reduction in its sideband intensities at higher spinning speeds. Peak areas for the 0.4% Fe-forsterite (Table 4) sample are reported but no spectrum is presented as it resembles that of the 0.05% sample .

The spectrum of 0.1% Fe-monticellite (Fig. 5, Table 5) displays 7 paramagnetically shifted peaks. The peaks have similar line shapes and widths and nearly equal areas within experimental uncertainty. Four peaks appear at higher frequencies, peak 1 isolated at +22.3 ppm, peaks 2 and 3 slightly overlapping at +11.4 ppm and +8.8 ppm respectively, and peak 4 forming a shoulder on the main peak at +3.2 ppm. At lower frequencies, peaks 7 and 6 are clearly separated at -28.5 ppm and -19.6 ppm respectively, and peak 5 is at -6.1 ppm, between the resonance for the akermanite impurity and the unshifted monticellite peak.

315 **Co-containing samples**

316 Figure 3 shows the ^{29}Si NMR spectrum of ^{29}Si-enriched, 0.1% Co-forsterite (Table 6)
317 which exhibits 26 paramagnetically shifted peaks. This sample was reported on previously in
318 Stebbins et al. (2009a,b) as "Fo-1", but new, higher quality data were collected to better resolve
319 the shifted peaks. The ^{29}Si enrichment gives a much higher signal to noise ratio in which a peak
320 with 0.04% intensity should be detectable. 14 peaks are shifted up in frequency by as much as
321 +36.8 ppm and 12 are shifted down in frequency as much as -61.7 ppm, exceeding the
322 maximum shifts seen in the Fe-spectra. Peak areas are not as evenly distributed as in the
323 spectra for the Fe-forsterite, with some range of peak sizes. Figure 6 displays the spectrum of
324 isotopically normal 0.65% Co-forsterite, shifted by -4.1 ppm to allow more direct comparison
325 with Co-monticellite data. There are approximately 7 peaks visible and multiple shoulders. At
326 this higher concentration the broadening caused by the Co^{2+} obscures the fine features of the
327 individual paramagnetically shifted peaks and at even higher concentrations (greater than 1%
328 Co) the remaining features become unresolvable. As for Ni-containing samples, the spectra of
329 the Co-bearing, sol-gel forsterites showed parmagnetically shifted peaks that were similar to
330 those described here for the higher-Co samples made by sintering of oxides, but were not
331 analyzed in detail because of heterogeneity.

332 Figure 6 also displays the 0.25% Co-monticellite spectrum (Table 7) which contains 3
333 labeled paramagnetically shifted peaks. The two higher frequency peaks at +17.6 ppm and
334 +10.5 ppm overlap significantly with the unshifted peak due to their relative inward shift and to
335 peak broadening. Peak 3 is shifted far down in frequency, by -44.3 ppm. An unshifted
336 akermanite impurity peak is again present at -72.0 ppm.

Undoped, Cu- and Mn-bearing forsterite and San Carlos olivine

Spectra of Mn-bearing forsterites, even at the 0.1% concentration level, display drastic peak broadening (10 to 20 times that of comparable levels of Ni, Co or Fe^{2+}), which prevented the identification of any paramagnetically shifted peaks (Fig. 8). This is probably the result of an unusually large effect on relaxation: unlike the other samples, the entire observed peak was fully relaxed at the short pulse delay of 0.05 s (Table 1), with no improvement in resolution at longer delays. Unfortunately, this severe broadening prevents any analysis of Mn^{2+} site occupancies, which are expected to be different from other cations described here.

Our attempts to add significant concentrations of Cu^{2+} to forsterite were unsuccessful, yielding undetectable dopant levels and no effects on NMR spectra, presumably due to the ease of reduction of this cation to Cu^{1+} (diamagnetic) and even Cu^{0} at high temperature synthesis conditions.

Spectra of undoped forsterite samples also presented very small paramagnetically shifted peaks at the same positions as some of those observed in Co- and Ni-bearing samples, most likely the result of minor cross-contamination from Pt crucibles, which can readily alloy with these metals. This same scenario is likely the source of Co contamination identified (via the observation of tiny paramagnetically shifted peaks) in the “Fo-unen” and “Fo-noCo” samples of Stebbins et al. (2009a,b).

As already described in the early days of high resolution, solid state NMR (Grimmer et al. 1983), the ^{29}Si spectrum of San Carlos olivine is so severely broadened by its high Fe^{2+} content (about 10% Fe in the notation used here, or approximately Fo_{90}) as to be difficult to

358 observe, with little structurally useful information (Fig. 8). Only the broad (55 ppm) central
359 resonance is shown here, not the accompanying wide manifold of spinning sidebands, which is
360 particularly intense for this sample.

361 **Discussion**

362 The positions of the paramagnetically shifted peaks observed in the ^{29}Si NMR spectra
363 are expected to be highly sensitive to variations in geometric relationships (number of
364 separating bonds, distances, angles, and accompanying changes in electronic structure)
365 between the paramagnetic transition metal cation and the ^{29}Si nucleus (Grey et al. 1989, 1990;
366 Palke and Stebbins 2011a, 2011b). Multiple peaks are present due to the various possible
367 configurations. In order to make sense of the observed peak shifts, we must carefully examine
368 the well-known forsterite structure. Table 8 lists M1 and M2 sites that are 2 bonds (first cation
369 shell) or 4 bonds (second cation shell) away from a central silicon site, as well as the M1-Si or
370 M2-Si distances (Fujino et al. 1981). The expected relative areas of shifted peaks resulting from
371 the substitution of paramagnetic cations into each configuration, based simply on the numbers
372 of geometrically equivalent sites, are also given. The Si atom lies on a mirror plane; the first and
373 second neighbor M1 sites are all off the mirror plane and occur in groups (e.g. the first
374 neighbor, edge shared site at 2.695 Å or the second neighbor site at 4.412 Å) each with two
375 symmetrically equivalent M1-Si configurations. Therefore, transition metal cations occupying
376 M1 sites should produce several peaks of *equal* area. The first- and second-neighbor M2 sites to
377 the Si can be either off or on the mirror plane and thus occur in groups each with either one or
378 two symmetrically equivalent M2-Si configurations. This will produce paramagnetically shifted

peaks of *unequal* area with some having twice the intensity as others. The peak area for a given M1-Si or M2-Si configuration will be proportional to the concentration of the transition metal cation on the M1 or M2 sites, denoted X or Y, respectively. Peak areas are then dependent on whether the M site lies on the same mirror plane as Si. For example, a shifted peak related to an off-mirror plane M2 site will have an intensity of 2Y while the on-mirror plane M2 site will have an intensity of Y (Table 8). Measured peak areas can be compared to this tabulation and thus yield information about the site preference of the paramagnetic cation for M1 or M2. As a first approximation, a paramagnetic cation closer to the observed silicon should produce a frequency shift with a greater magnitude (possibly either up or down in frequency), although a simple proportionality between distance and shift is not expected if the through-bond "Fermi contact shift" mechanism is predominant.

We note that the distributions of transition metal cations on the M1 and M2 sites in olivine are known to depend on temperature (Heinemann et al. 2007), although detection of such effects by the methods described here would require especially high-quality spectra. The rate-dependent "closure temperatures" for ordering of cations during cooling, at which site occupancies are quenched in, may be well below the synthesis temperatures used here, but are not precisely known, especially for Co- and Ni-containing olivines.

Ni-forsterite and monticellite

The uniform intensities of peaks 7, 9, 10 and 11 in the spectra for the Ni-forsterite samples agree well with an M1-only site occupancy, and thus requires paramagnetic shift contributions from at least some sites that are 4 bonds away as there are only two distinct M1-

Si configurations within 2 bonds. Similar conclusions were reached in our recent studies of pyrope-rich garnets (Palke et al., submitted). From Table 8, nine paramagnetically shifted peaks might be expected from sites within this range. While only four shifted peaks are clearly resolved, additional peaks are likely to contribute to the spectra but may be shifted such small distances that they cannot be resolved from the main, unshifted peak (e.g. a shoulder seen just above peak 11 in the 0.25% Ni-forsterite). For example, the four M1 second-neighbor sites at distances greater than 6 Å might be expected to give especially small shifts. The paramagnetically shifted peaks seen in the Ni-forsterite spectra have corresponding locations in the 1% Ni-monticellite spectra (Fig. 4). The correlation between the peak positions in the two phases is near linear, a trend that is not necessarily anticipated for paramagnetic shifts, but is likely to be related to the larger unit cell and longer average bond distances in monticellite (Fig. 9) . Ni-monticellite peak 2 appears to be the result of two overlapping peaks corresponding to Ni-forsterite peaks 9 and 10. Its area is 30% larger than expected using peaks 1 and 3 as references, but this is probably within experimental error, based on comparisons of nominally "equal area" peaks in other spectra. Due to the large difference in ionic radii between Ni^{2+} and Ca^{2+}, Ni^{2+} is expected to occupy only the M1 site in monticellite with full occupation of M2 by Ca. Therefore, the similarity of the monticellite and forsterite spectra confirm that Ni^{2+} in forsterite occupies solely the M1 site. Most importantly, the assumption that the monticellite spectrum should closely match the forsterite M1 features seems robust, which proves very useful for the analysis of the Fe- and Co-forsterites below.

The additional paramagnetically shifted peaks for the 5% Ni-Forsterite sample (peaks 1-5, 8, Fig. 1) match the expected locations and peak areas of combination peaks for Si sites with

two or three Ni^{2+} cation M1 neighbors. These combination peaks should be found at positions approximately equal to the sum of the two or three individual shifts, and with areas proportional to the probability of having two or three such neighbors (Grey et al. 1989, 1990; Palke and Stebbins 2011b; Palke et al. submitted). Assuming a random distribution of Ni^{2+} on M1 sites, the probability of various Ni-Si configurations can be predicted. Peaks 7, 9 10, and 11 are each due to a single Ni^{2+} cation neighbor, as evidenced by their presence in the spectrum for the lowest Ni^{2+} concentration, allowing the location of double- and triple-neighbor shifted peaks to be calculated as sums of these single neighbor positions. The expected peak areas and locations are in good agreement with the measured spectrum (Figure 10, discussed below). The largest deviation between the prediction and observation is for peak 8, which is 4% larger than predicted from the overlap of combination peaks 7+11 and 9+10 that add up to make this combination resonance. The peak locations of the farthest-shifted double and triple combination peaks deviate somewhat from the prediction, such as peak 3 which is shifted by +1.7 ppm further than predicted by the sum of shifts for 7 and 7 (44.0 vs. 42.3). This is likely because the incorporation of two Ni^{2+} cations in adjacent sites causes small structural distortion resulting in changes to the paramagnetic shifts.

To illustrate this approach for the 1% and 5% Ni-forsterites, we have simulated spectra assuming random distributions of Ni^{2+} (on M1 sites only) to predict relative areas of shifted peaks. We fit peak widths and positions to those of the singly-shifted resonances, then predict the doubly-and triply-shifted peaks with areas proportional to the probabilities of two or three Ni^{2+} neighbors and shifts that are sums of corresponding single shifts. Results are shown in Figure 10, and match the experimental spectra remarkably well. Triply-shifted peaks are in

general too small for ready detection, as are some doubly-shifted peaks, but in total are a significant part of the overall intensity, accounting for roughly 7%. The absence of any obvious deviations from peak intensities given by this random model prediction suggest that strong localized clustering of Ni^{2+} or significant Ni^{2+} occupancy of M2 are unlikely.

As mentioned in the introduction and discussed at some length in recent studies of garnets and monazites (Palke and Stebbins 2011a; Palke and Stebbins 2011b, Palke et al. 2013; Palke et al., submitted), as well as in pioneering earlier work on yttrium and tin-containing pyrochlore phases (Grey et al. 1989, 1990), both through-bond electronic structure effects (Fermi contact shift) and through space dipolar couplings from asymmetric sites (not fully averaged in MAS NMR, the "pseudo-contact" shift) can result in paramagnetic shifts of NMR resonances. Both can contribute significantly, but distinguishing between the two mechanisms can be difficult. Fortunately, detailed studies of a Ni-bearing forsterite single crystal yielded a quantitative description of the angular dependence and asymmetry of the EPR spectrum resulting from its unpaired electron spins (the "g-tensor"), as well as confirming the M1 site occupancy (Rager et al. 1988). This information, and the equations for calculating pseudocontact shifts given by Bertini et al. (2002) were used to estimate the maximum range of possible pseudocontact shifts. If only the latter peaks were present, the maximum shift distance would be only 2.1 to -0.6 ppm, which would make them unresolvable from the main unshifted peak. This indicates that the resolvable paramagnetically shifted peaks in the spectra of the Ni-forsterites described here must be primarily the products of the Fermi contact interaction.

464 **Fe-forsterite and monticellite**

465 The number of observed peaks in the spectra of Fe-forsterite samples is dramatically
466 greater than for the Ni-forsterites and immediately indicates a different site distribution for
467 Fe^{2+}. The relatively large variations in peak areas suggests as well that M2 sites are occupied as
468 well as M1, as the former can vary depending on local symmetry (Table 8). Peaks 6, 7, 8, 9, 10,
469 and 11 overlap with the unshifted peak or with each other, and their peak areas cannot be well
470 constrained, making them unsuitable for use in an analysis of site occupancies. In contrast,
471 peaks 1, 2, 3, 4, 5, 12, 13 14, 15 and 16 can be resolved and fit with a higher degree of certainty.
472 However, the areas of even this subset of peaks cannot be easily divided into groups, so
473 identifying site occupancy based on peak areas is difficult. Additionally, if there is a nearly equal
474 ratio of Fe^{2+} on M1 to M2, as expected from previous studies of Fe-rich olivines, peaks in the
475 silicon spectrum resulting from M1 and M2 occupancies would not be readily distinguishable
476 (i.e. X and Y in Table 8 would have similar values).

477 However, comparison of Fe-forsterite to Fe-monticellite (Fig. 5) does allow some
478 separation of M1 or M2 peaks in the forsterite spectrum. Monticellite peaks 6 and 7 appear to
479 closely correlate to forsterite peaks 15 and 16. Indeed, a plot of the Fe-forsterite vs. Fe-
480 monticellite peak positions again shows a strong linear correlation between Fe-forsterite peaks
481 3, 5, 8, 15, and 16 and Fe-monticellite peaks 1, 3, 4, 6, and 7. Additionally, Fe-forsterite peaks 4
482 and 12 linked to Fe-monticellite peaks 2 and 5 lie close to this linear trend. Figure 9 plots the
483 identified corresponding peaks of the Ni^{2+}, Fe^{2+}, and Co^{2+} illustrating the linear relationship
484 between the forsterite and monticellite M1 paramagnetic shifts. An additional method of
485 determining peak assignments can be developed by considering peak areas. At the expected

positions of Fe-forsterite peaks 1, 2 and 3 only one peak can be found in the Fe-monticellite spectrum indicating that two of these are caused by Fe^{2+} in M2 in the former. Since some of the M2 sites lie on the same mirror plane as the Si and some are off the plane, we expect two groups of peaks for Fe^{2+} in M2, with some peaks having half the area of the others. Fe-forsterite peak 1 is close to half the size of peaks 2 or 3, and the presence of only one monticellite peak in this region of the spectrum indicates that peaks 2 and 3 must correspond to silicon sites with neighboring occupied M1 and M2 off-mirror plane sites. Using areas of Fe-forsterite peaks 1, 2 and 3 the distribution was determined as 48±23% M1, which closely matches the roughly 1:1 distribution expected from data on high Fe olivines.

Peak areas were predicted using Fe concentrations given by EPMA and the assumption of a 1:1, random distribution of Fe^{2+} on M1 and M2. In the 0.05% Fe-forsterite, M1 and M2 off-mirror plane peaks should each have areas of 0.2% and M2 on-mirror plane peaks should have areas of 0.1%. There are some peaks near each of these predicted areas, but the majority of the peaks are between the two predicted values, suggesting that experimental precision is not good enough to make this distinction. In the 0.4% Fe-forsterite sample, M1 and M2 off-mirror planes area predictions are 1.2% and M2 on-mirror plane peak areas are 0.6%, which are again similar to the observed range of areas.

Although the Fe-bearing samples were not as homogeneous and their spectra were not as well resolved as the Ni-bearing samples and spectra, attribution of features in the silicon spectra to M1 or M2 site occupation is still possible and is consistent with expectations from Fe-rich olivines. While measured peak areas do not fit completely with the peak assignment model

developed above, probably because of experimental imprecision, two lines of research could confirm this analysis. As discussed by Middlemiss et al. (2013), DFT calculations are beginning to provide insights into specific peak assignments to interactions between paramagnetic cations and NMR nuclides. Additionally, ^{29}Si-enriched samples could increase signal to noise in the spectra and improve the precision of measured intensities of the paramagnetically shifted peaks

Co forsterite and monticellite

The analysis of the ^{29}Si NMR spectrum of the 0.1% Co-forsterite is made more precise by the higher signal to noise ratio resulting from its isotopic enrichment, yielding more complete information about Co^{2+} site preference. This spectrum displays a large number of peaks indicating that Co^{2+} is present (in some ratio) on both M1 and M2 sites, as in Fe-forsterite. These can be separated into groups based on their relative areas (Table 6): group A with the smallest areas ranging from 0.01 to 0.018% (peaks 1, 4, 7, 8, 22, 23, and 24), group B with distinctly larger areas from 0.027% to 0.055% (peaks 2, 5, 18, 21, and 25), group C ranging from 0.086% to 0.114% (peaks 3, 6, 17, 19, 20, and 26), and group D comprising those with areas above 0.135% (peaks 10, 12, 13, 14, 15, and 16). Several studies of olivines with much higher Co concentrations have suggested a significant, but not exclusive, preference for M1 over M2 (Müller-Sommer et al. 1997; Taran and Rossman 2001). A similar site distribution at low Co^{2+} concentrations would suggest that paramagnetically shifted peaks related to Co^{2+} in M1 should be systematically larger than those related to M2. Group A can therefore be expected to contain the shifts caused by Co^{2+} in M2 on the mirror plane with Si. The average area of the group B peaks is approximately twice that for group A, so group B may represent the signals

529 from Co^{2+} in off-mirror plane M2 sites. The much larger peaks in group C then are likely to be
530 contributions from Co^{2+} in M1 sites.

531 These assignments can be at least partially corroborated by comparing the spectrum of
532 Co-monticellite to that of 0.65% Co-forsterite, where peak numbers correspond to those in the
533 lower-dopant sample (Fig. 6). Here, the paramagnetically shifted peaks for the Co-monticellite
534 can be assumed to be caused by Co^{2+} in the M1 sites only. Co-forsterite peak 26 appears to
535 correspond to Co-monticellite peak 3 since there is little else in this region of the spectra, and
536 peaks 1 and 2 for the Co-monticellite appear to correspond to Co-forsterite peaks 3 and 6 (Fig.
537 6, dashed lines). As for Fe-forsterite and monticellite, there is rough linear correlation between
538 the shifts of the observable, corresponding M1 peaks in the Co-forsterite and Co-monticellite,
539 with systematically smaller shifts in the latter (Fig. 9). In the higher-resolution spectrum for the
540 0.1% Co-forsterite (Fig. 3), the areas of peaks of 3, 6 and 26, are all of similar area and are larger
541 than other neighboring peaks. Thus peaks 3, 6 and 26 are assigned as signals resulting from
542 silicon sites with neighboring Co^{2+} in M1. This analysis thus also supports our assumption that
543 the small area peaks, group A and group B, in the 0.1% Co-forsterite spectrum are caused by
544 Co^{2+} in M2.The larger-area group D peaks, which are the least shifted and least well-resolved,
545 probably each contain multiple overlapped contributions and cannot readily be assigned: single
546 peaks of much larger areas than those in group C are not expected from our analysis of the
547 structure. However, with multiple, clearly identified contributions from Co^{2+} in both M1 and M2
548 sites, averages of the peak areas for groups A, B and C can be compared to determine the site
549 preference for Co^{2+}. Using the symmetry-constrained relationship between intensities for on-
550 mirror-plane M1 and M2 site peaks, 2X and 2Y, respectively, a 76±12% M1 site preference can

be determined for Co^{2+} in forsterite. Müller-Sommer et al. (1997) determined the Co^{2+} preference for the M1 site with an X-ray Rietveld analysis of a series of olivines ranging from $(Co_{0.13}Mg_{0.87})_2SiO_4$ to Co_2SiO_4, all equilibrated at 1200 ˚C and cooled to room temperature within two minutes. At the Co^{2+} concentrations of our forsterite samples, an 84% M1 site preference is predicted by their results, which agrees well with our determined value.

Implications

The ^{29}Si spectra of forsterite containing 0.05 to 5% of Ni^{2+}, Co^{2+}, and Fe^{2+} display large numbers (4 to 26 or more) of resolvable resonances caused by interactions of unpaired electron spins with nuclear spins. These potentially contain a wealth of information about site occupancies, short range order/disorder, and substitution mechanisms, as has begun to be reported for other minerals such as garnets and REE phosphates. Although we cannot yet fully analyze these spectra (a task that probably awaits the development and application of advanced theoretical methods), partial analysis gives reasonable assignments of peaks to each different cation in either exclusively M1 sites (Ni^{2+}), roughly equal occupancy in both M1 and M2 (Fe^{2+}), or both sites with a strong preference for M1 (Co^{2+}). Comparison to analogous Ni-bearing monticellite samples, where M1-only occupancies are expected, helps confirm these assignments. These site preferences agree well with those predicted by previous studies of olivines with higher transition metal cation concentrations, suggesting some simplicity to controlling mechanisms of solution. Future NMR studies seeking to investigate the effects of temperature and composition on M1/M2 ordering in olivines with relatively low transition metal cation contents would require high quality spectra to tightly constrain peak areas. ^{29}Si

572 enriched samples would be very useful in detecting small (approximate 5% or less) changes in
573 paramagnetically shifted peak areas anticipated by the findings and analysis of higher
574 concentration studies (Kroll et al. 2006; Morozov et al. 2006; Heinemann et al. 2007). If
575 detectable, these results could be important complements to existing data from XRD and other
576 methods on samples with higher concentrations, to better refine solution models.

577 The approach chosen here of keeping magnetic dopant ion levels low enough to avoid
578 problematic line broadening, as well as comparing effects of cations expected to have different
579 site occupancies, suggests the possibility of application to other problems of short-range
580 structure in silicate and other minerals and related technological materials; the documentation
581 of shifted NMR peaks for one, two, and even three paramagnetic cation neighbors provides
582 prospects for unique opportunities to detect cation clustering, as was noted in early studies of
583 pyrochlore phases (Grey et al. 1989, 1990). In minerals such as forsterite that can have very
584 narrow NMR peaks, effects of paramagnetic cations can be detected at very low concentrations
585 (< 0.1%) even in isotopically normal samples, if experiments are done with very rapid pulsing to
586 enhance these fast-relaxing signals. ^{29}Si enrichment can increase this sensitivity even more.

587 Broadening effects, as shown here for low concentrations of Mn^{2+} and high
588 concentrations of Fe^{2+} in olivine, may still produce NMR spectra that are unresolved and which
589 appear to retain little structural information. However, results presented here suggest that
590 even in such systems, future NMR studies could prove interesting, perhaps if conducted with
591 very rapid sample spinning rates (now possible up to >100 kHz in some cases) or at low

592 temperatures where separation due to paramagnetic shifts may be much greater and
593 relaxation times altered.

594

595 **Acknowledgements**

596 This research was supported by NSF grant EAR-1019596 to J.F.S. We thank Suzie S. Rigby (Brock
597 University) who synthesized the sol-gel samples with financial support by the Natural Sciences
598 and Engineering Research Council of Canada (NSERC), and Bob Jones (Stanford) for assistance
599 with EPMA analyses.

600

601

602 ## References

603 Bégaudeau, K., Morizet, Y., Paris, M., Florian, P., Léveque, F., and Mercier, J.C. (2009)
604 Quantitative analysis of hydroxyl ions in pyroxenes from Kilbourne Hole peridotites (New
605 Mexico): an FTIR and NMR study. American Geophysical Union, Fall Meeting, abstract
606 MR43A–1868.

607 Bégaudeau, K., Morizet, Y., Florian, P., Paris, M., and Mercier, J.-C. (2012) Solid-state NMR
608 analysis of Fe-bearing minerals: implications and applications for Earth sciences. European
609 Journal of Mineralogy, 24, 535–550.

610 Bertini, I., Luchinat, C., and Parigi, G. (2002) Magnetic susceptibility in paramagnetic NMR.
611 Progress in Nuclear Magnetic Resonance Spectroscopy, 40, 249–273.

612 Brown, G.E. (1980) Olivines and Silicate spinels. In: Reviews in Mineralogy and Geochemistry,
613 Vol. 5, pp. 275–381.

614 Canil, D. (1994) An experimental calibration of the “Nickel in Garnet” geothermometer with
615 applications. Contributions to Mineralogy and Petrology, 117, 410–420.

616 Fujino, K., Sasaki, S., Takéuchi, Y., and Sadanaga, R. (1981) X-ray determination of electron
617 distributions in forsterite, fayalite and tephroite. Acta Crystallographica, B37, 513–518.

618 Ghose, S., and Wan, C. (1974) Strong site preference of Co^{2+} in olivine, $Co_{1.10}Mg_{0.90}SiO_4$.
619 Contributions to Mineralogy and Petrology, 47, 131–140.

620 Grey, C.P., and Dupré, N. (2004) NMR studies of cathode materials for lithium-ion rechargeable
621 batteries. Chemical Reviews, 104, 4493–4512.

622 Grey, C.P., Dobson, C.M., Cheetham, A.K., and Jakeman, R.J.B. (1989) Studies of rare-earth
623 stannates by tin-119 MAS NMR. The use of paramagnetic shift probes in the solid state.
624 Journal of the American Chemical Society, 111, 505–511.

625 Grey, C.P., Smith, M.E., Cheetham, A.K., Dobson, C.M., and Dupree, R. (1990) Yttrium-89 MAS
626 NMR study of rare-earth pyrochlores: paramagnetic shifts in the solid state. Journal of the
627 American Chemical Society, 112, 4670–4675.

628 Grimmer, A.R., von Lampe, F., Magi, M., and Lippmaa, E. (1983) High resolution ^{29}Si NMR of
629 solid silicates: influence of Fe^{2+} in olivines. Zeitschrift fur Chemie, 23, 343–344.

Harris, P.G., Reay, A., and White, I.G. (1967) Chemical composition of the upper mantle. Journal of Geophysical Research, 72, 6359–6369.

Hartman, J.S., Narayanan, A., Rigby, S.S., Sliwinski, D.R., Halden, N.M., and Bain, A.D. (2007) Heterogeneities in sol-gel-derived paramagnetics-doped forsterites and willemites – Electron microprobe analysis and stretched-exponential ^{29}Si MAS NMR spin-lattice relaxation studies. Canadian Journal of Chemistry, 65, 56–65.

Heinemann, R., Kroll, H., Kirfel, A., and Barbier, B. (2007) Order and anti-order in olivine III: Variation of the cation distribution in the Fe,Mg olivine solid solution series with temperature and composition. European Journal of Mineralogy, 19, 15–27.

Henderson, C.M.B., Redfern, S.A.T., Smith, R.I., Knight, K.S., and Charnock, J.M. (2001) Composition and temperature dependence of cation ordering in Ni-Mg olivine solid solutions: a time-of-flight neutron powder diffraction and EXAFS study. American Mineralogist, 86, 1170–1187.

Kroll, H., Kirfel, A., and Heinemann, R. (2006) Order and anti-order in olivine II: Thermodynamic analysis and crystal-chemical modelling. European Journal of Mineralogy, 18, 691–704.

Lee, Y.J., Wang, F., and Grey, C.P. (1998) ^{6}Li and ^{7}Li MAS NMR studies of lithium manganate cathode materials. Journal of the American Chemical Society, 120, 12601–12613.

Loucks, R.R. (1996) A precise olivine-augite Mg-Fe-exchange geothermometer. Contributions to Mineralogy and Petrology, 125, 140–150.

Mägi, M., Lippmaa, E., Samoson, A., Engelhardt, G., and Grimmer, A.R. (1984) Solid-state high-resolution silicon-29 chemical shifts in silicates. The Journal of Physical Chemistry, 88, 1518–1522.

McCarty, R.J., Palke, A.C., Stebbins, J.F., and Hartman, J.S. (2012) A ^{29}Si MAS-NMR study of transition metal site occupancy in forsterite. American Geophysical Union, Fall Meeting, abstract MR11A–2470.

McCarty, R.J., Palke, A.C., and Stebbins, J.F. (2014) The site preference and distribution of low concentration elements in forsterite as determined by NMR. 2014 Goldschmidt Conference, Abstracts, 1638.

McCormick, T.C., Smyth, J.R., and Lofgren, G.E. (1987) Site occupancies of minor elements in synthetic olivines as determined by channeling-enhanced X-ray emission. Physics and Chemistry of Minerals, 14, 368–372.

Middlemiss, D.S., Ilott, A.J., Clément, R.J., Strobridge, F.C., and Grey, C.P. (2013) Density functional theory-based bond pathway decompositions of hyperfine shifts: Equipping

663 solid-state NMR to characterize atomic environments in paramagnetic materials.
664 Chemistry of Materials, 25, 1723–1734.

665 Morozov, M., Brinkmann, C., Grodzicki, M., Lottermoser, W., Tippelt, G., Amthauer, G., and
666 Kroll, H. (2006) Octahedral cation partitioning in Mg,Fe^{2+}-olivine. Mössbauer spectroscopic
667 study of synthetic $(Mg_{0.5}\ Fe^{2+}_{0.5})_2SiO_4$ (Fa_{50}). Hyperfine Interactions, 166, 573–578.

668 Müller-Sommer, M., Hock, R., and Kirfel, A. (1997) Rietveld refinement study of the cation
669 distribution in (Co, Mg)-olivine solid solution. Physics and Chemistry of Minerals, 24, 17–
670 23.

671 Nielsen, U.G., Paik, Y., Julmis, K., Schoonen, M.A., Reeder, R.J., and Grey, C.P. (2005)
672 Investigating sorption on iron-oxyhydroxide soil minerals by solid-state NMR spectroscopy:
673 a ^{6}Li MAS NMR study of adsorption and absorption on goethite. The Journal of Physical
674 Chemistry. B, 109, 18310–18315.

675 Palke, A.C., and Stebbins, J.F. (2011a) Paramagnetic interactions in the ^{31}P NMR spectroscopy of
676 rare earth element orthophosphate ($REPO_4$, monazite/xenotime) solid solutions. American
677 Mineralogist, 96, 1343–1353.

678 ——— (2011b) Variable-temperature ^{27}Al and ^{29}Si NMR studies of synthetic forsterite and Fe-
679 bearing Dora Maira pyrope garnet: Temperature dependence and mechanisms of
680 paramagnetically shifted peaks. American Mineralogist, 96, 1090–1099.

681 Palke, A.C., Stebbins, J.F., Frost, D.J., and McCammon, C.A. (2012) Incorporation of Fe and Al in
682 $MgSiO_3$ perovskite: An investigation by ^{27}Al and ^{29}Si NMR spectroscopy. American
683 Mineralogist, 97, 1955–1964.

684 Palke, A.C., Stebbins, J.F., and Boatner, L.A. (2013) ^{31}P magic angle spinning NMR study of flux-
685 grown rare-earth element orthophosphate (monazite/xenotime) solid solutions: evidence
686 of random cation distribution from paramagnetically shifted NMR resonances. Inorganic
687 chemistry, 52, 12605–12615.

688 Palke, A.C., Stebbins, J.F., Geiger, C.A., and Tippelt, G. (in press) Cation order-disorder in Fe-
689 bearing pyrope and grossular garnets: An ^{27}Al and ^{29}Si MAS NMR and ^{57}Fe Mössbauer
690 spectroscopy study. American Mineralogist.

691 Rager, H., Hosoya, S., and Weiser, G. (1988) Electron paramagnetic resonance and polarized
692 optical absorption spectra of Ni^{2+} in synthetic forsterite. Physics and Chemistry of Minerals,
693 15, 383–389.

694 Rajamani, V., Brown, G.E., and Prewitt, C.T. (1975) Cation Ordering in Ni-Mg Olivine. American
695 Mineralogist, 60, 292–299.

Stebbins, J.F. (1995) Nuclear magnetic resonance spectroscopy of silicates and oxides in geochemistry and geophysics. In: Ahrens, T. (Ed.) A Handbook of Physical Constants, AGU Reference Shelf 2 pp. 303–331. American Geophysical Union.

Stebbins, J.F., and Kelsey, K. (2009) Anomalous resonances in ^{29}Si and ^{27}Al NMR spectra of pyrope ($Mg_3Al_2Si_3O_{12}$) garnets: effects of paramagnetic cations. Physical Chemistry Chemical Physics, 11, 6906–6917.

Stebbins, J.F., and Xue, X. (2014) NMR Spectroscopy of Inorganic Earth Materials. Reviews in Mineralogy and Geochemistry, 78, 605–653.

Stebbins, J.F., Smyth, J.R., Panero, W.R., and Frost, D.J. (2009a) Forsterite, hydrous and anhydrous wadsleyite and ringwoodite (Mg_2SiO_4): ^{29}Si NMR results for chemical shift anisotropy, spin-lattice relaxation, and mechanism of hydration. American Mineralogist, 94, 905–915.

Stebbins, J.F., Panero, W.R., Smyth, J.R., and Frost, D.J. (2009b) Forsterite, wadsleyite, and ringwoodite (Mg_2SiO_4): ^{29}Si NMR constraints on structural disorder and effects of paramagnetic impurity ions. American Mineralogist, 94, 626–629.

Taftø, J., and Spence, J.C. (1982) Crystal site location of iron and trace elements in a magnesium-iron olivine by a new crystallographic technique. Science, 218, 49–51.

Taran, M., and Rossman, G. (2001) Optical spectra of Co^{2+} in three synthetic silicate minerals. American Mineralogist, 86, 889–895.

Wu, C.M., and Zhao, G.C. (2007) A recalibration of the garnet-olivine geothermometer and a new geobarometer for garnet peridotites and garnet-olivine-plagioclase-bearing granulites. Journal of Metamorphic Geology, 25, 497–505.

719 **List of figure captions**

720 **Figure 1**. ^{29}Si MAS NMR spectra at 9.4 T (5% and 0.25%) or 14.1 T (1%), 0.05 s pulse delay, of
721 forsterite with three different Ni concentrations, with spinning speeds 15 kHz (5% and 0.25%)
722 and 20 kHz (1%). The lower three spectra are repeated above with their vertical scales enlarged
723 as indicated. Dashed lines are drawn between corresponding double neighbor
724 paramagnetically shifted peaks for samples with different Ni concentrations. * marks unknown
725 impurity phase. Here and in all other figures except Figure 7, all spinning sidebands are well
726 outside of the frequency range shown.

727 **Figure 2**. ^{29}Si MAS NMR spectra (14.1 T, 0.05 s pulse delay) of Fe-forsterite at two spinning
728 speeds as shown, illustrating effects of air frictional heating on positions of paramagnetically
729 shifted peaks.

730 **Figure 3**. ^{29}Si MAS NMR spectrum (14.1 T, 0.05 s pulse delay) of ^{29}Si enriched forsterite with
731 0.1% Co at 20 kHz spinning speed.

732 **Figure 4.** ^{29}Si MAS NMR spectra (9.4 T, 0.05 s pulse delay) of 1% Ni-monticellite and 1% Ni-
733 forsterite both at 15 kHz spinning speed. In the former, the akermanite impurity is labeled with
734 "ak" and an unknown impurity phase with an asterisk. The Ni-forsterite spectrum is shifted -4.1
735 ppm to align with the unshifted peak of the Ni-monticellite. Dashed lines are drawn between
736 corresponding peaks.

737 **Figure 5**. ^{29}Si MAS NMR spectra (14.1 T, 0.05 s pulse delay) of Fe-monticellite and Fe-forsterite
738 at spinning speeds of 20 kHz. In the Fe-monticellite, the akermanite impurity is labeled as "ak".

739 The Fe-forsterite spectrum is shifted -4.1 ppm to align with the unshifted peak of the Fe-
740 monticellite peak. Dashed lines are drawn between corresponding peaks.

741 **Figure 6**. ^{29}Si MAS NMR spectra (14.1 T, 0.05 s pulse delay, 20 kHz spinning speed) of Co-
742 monticellite and Co-forsterite. The akermanite impurity phase is labeled as "ak". The Co-
743 forsterite spectrum is shifted -4.1 ppm to align with the unshifted Co-monticellite peak. Dashed
744 lines mark corresponding peaks.

745 **Figure 7.** ^{29}Si MAS NMR spectrum of 0.05% Fe-forsterite (as in Fig. 1), comparing the central
746 band of peaks to the first group of spinning side bands to higher frequency, shifted in frequency
747 by -101 ppm. Note the greatly reduced relative intensity of the unshifted resonance in the
748 latter, allowing improved resolution of at least one close-in shifted peak (#9).

749 **Figure 8.** ^{29}Si MAS NMR spectrum (14.1 T, 0.05 s pulse delay) of Mn-forsterite, showing severe
750 line broadening effects of Mn^{2+}. A spin-echo MAS spectrum of San Carlos olivine (9.4 T, 10 kHz
751 spinning speed) is shown to illustrate broadening caused by a much higher Fe^{2+} content. In the
752 latter, the spike at 0 ppm is an artifact, and the inner edges of the first spinning sidebands can
753 be seen in the baseline.

754 **Figure 9.** A plot of paramagnetic shifts, relative to the central resonance, for peaks in
755 transition-metal containing forsterite and the corresponding ones in monticellite. Data shown
756 are from spectra collected at 14.1 T and 20 kHz spinning speed.

757 **Figure 10.** Observed ^{29}Si MAS NMR spectrum of 5% Ni-forsterite (as in Fig. 1), compared with
758 model that assumes random distribution of Ni^{2+} on M1 sites only.

759

760 **Table 1.** Sample compositions and data on ^{29}Si MAS NMR spectra of main, unshifted peaks.

Name[a]	Dopant conc. (apfu)[b]	FWHM (ppm)	Line shape[d]	% relaxed[e]
0.1% Mn-forsterite	0.002[c]	27.3	-	100%
0.05% Fe-forsterite	0.001 (1)	2.1	0.30	14%
0.4% Fe-forsterite	0.008 (24)	2.2	0.40	51%
San Carlos Olivine	0.20 (2)	55	-	100%
0.1% Fe-monticellite	0.002 (1)	1.1	0.00	11%
0.1% Co-forsterite	0.002 (0)	0.8	0.20	15%
0.65% Co-forsterite	0.013 (4)	1.1	0.00	17%
0.25% Co-monticellite	0.005 (2)	3.8	0.40	20%
0.25%Ni-forsterite	0.005 (1)	0.8	0.88	73%
1% Ni-forsterite	0.020 (0)	0.8	0.50	84%
5% Ni-forsterite	0.100 (3)	1.8	0.43	100%
1% Ni-monticellite	0.020 (3)	0.9	0.50	89%

761

762 [a] Based on ($Mg_{2-2x}M_{2x}SiO_4$) for forsterite, and ($CaMg_{1-2x}M_{2x}SiO_4$)for monticellite.

763 [b] Based on EPMA data, atoms per formula unit. Figures in parentheses show standard deviation
764 in analyses and indicate degree of sample homogeneity.

765 [c] Not analyzed, estimated by synthesis values.

766 [d] 1=100% Gaussian, 0=100% Lorentzian line shape for central, unshifted peak.

767 [e] % relaxation of unshifted peak at 0.05 s pulse delay, relative to full relaxation at long delays.

768

Table 2. Peak positions and areas for Ni-containing forsterite samples. "Source" shows origins of peaks that result from two or three Ni cations in sites that product the indicated single peaks.

	0.25%Ni-forsterite		1%Ni-forsterite		5%Ni-forsterite		
Peak	Shift (ppm)	Area (%)[a]	Shift (ppm)	Area (%)[b]	Shift (ppm)	Area (%)[c]	Peak source
1	-	-	-	-	51.9	0.1	7+7+9
2	-	-	-	-	48.8	0.1	7+7+10
3	-	-	-	-	44.0	0.4	7+7
4	-	-	-	-	35.6	0.3	7+9+10
5	-	-	-	-	29.6	1.7	7+9
6	-	-	-	-	26.7	1.3	7+10
7	20.8	0.8	21.6	3.2	20.9	9.9	-
8	-	-	-	-	14.4	4.1	7+11, and 9+10
9	8.4	0.7	8.6	3.3	8.4	9.5	-
10	5.8	0.7	6.0	3.4	5.8	9.0	-
Unshifted	0	97	0	87	0.0	47	-
11	-6.4	0.9	-6.9	3.3	-6.7	10.2	-

[a] uncertainty in area is about 26% relative.

[b] uncertainty in area is about 8% relative.

[c] Uncertainty in area is about 18% relative. Using the random model (see text),areas of doubly- and triply-shifted peaks within 35.5 to -6.7 ppm were estimated and account for 6.6% additional intensity, but are not listed individually.

778 **Table 3.** Peak positions and areas for 1% Ni monticellite.

	1% Ni-monticellite		corresponding
Peak	Shift (ppm)	Area (%)[a]	Ni-forsterite peak
1	14.2	3.3	7
2	3.1	7.9	9 and 10
Unshifted	0	86	
3	-3.1	2.7	11

779 [a] uncertainty in area is about 20% relative.

780

781 **Table 4.** Peak positions and areas for Fe^{2+}-containing forsterites.

	0.05% Fe-forsterite		0.4% Fe-forsterite		
Peak	Shift (ppm)	Area (%)[a]	Shift (ppm)	Area (%)[c]	Site[d]
1	38.7	0.13	35.2	0.5	M2
2	35.0	0.19	31.5	0.9	M2
3	30.3	0.18	27.5	0.9	M1
4	15.1	0.14	w/peak 5		M1
5	13.0	0.13	13.2	1.6	M1
6	9.7	0.40	w/peak 7		M2
7	8.2	0.12	8.3	4.1	M2
8	5.0	0.39	w/shoulder		M1
9	1.9	0.63[b]	w/shoulder		?
shoulder	ca. 1	0.10[b]	ca. 1	7.8	
unshifted	0	96	0	73	
shoulder	ca. -1.5	0.21[b]	ca. -1.5	5.8	
10	-5.2	0.09[b]	w/shoulder		?
11	-7.2	0.12[b]	w/shoulder		?
12	-10.4	0.17	-9.0	1.1	M1
13	-13.8	0.14	-12.4	0.7	M2
14	-19.2	0.13	-18.4	0.8	M2
15	-27.3	0.09	-22.8	0.9	M1
16	-39.1	0.19	-34.7	1.0	M1

782 [a] uncertainty in area is about 25% relative except as noted.

783 [b] less-resolved peak, uncertainty in area may be 25-50% relative.

784 [c] uncertainty in areas is about 17% relative.

785 [d] most likely location of Fe^{2+} cation responsible for observed peak.

786 **Table 5.** Peak positions and areas for 0.1% Fe-monticellite.

	0.1% Fe-monticellite		corresponding Fe-forsterite peak
Peak	Shift (ppm)	area (%)[a]	
1	22.3	0.4	3
2	11.4	0.3	4
3	8.8	0.5	5
4	3.2	0.5[b]	8
shoulder	ca. 1.5	2.0[b]	
unshifted	0	94	
shoulder	c.a. -2.5	1.0[b]	
5	-6.1	0.4[b]	12
6	-19.6	0.4	15
7	-28.5	0.5	16

787 [a] uncertainty in areas 21% relative, except as noted.

788 [b] less-resolved peaks, uncertainties 21-50% relative.

789

790 **Table 6.** Peak positions and areas for 0.1% Co-forsterite (95% ^{29}Si).

	0.1% Co-forsterite		
Peak	Shift (ppm)	Area (%)[a]	Site
1	36.8	0.010	M2-on-mirror
2	33.1	0.045	M2-off-mirror
3	31.0	0.113	M1
4	28.7	0.017	M2-on-mirror
5	21.7	0.027	M2-off-mirror
6	17.4	0.086	M1
7	14.3	0.014	M2-on-mirror
8	12.3	0.015	M2-on-mirror
9	10.2	0.05[b]	?
10	9.2	0.16[b]	?
11	7.7	0.01[b]	?
12	5.0	0.39[b]	?
13	3.9	0.17[b]	?
14	1.5	0.48[b]	?
unshifted	0	97.5	
15	-3.2	0.23[b]	?
16	-4.6	0.14[b]	?
17	-5.6	0.096	M1
18	-9.6	0.027	M2-off-mirror
19	-10.9	0.114	M1
20	-12.3	0.090	M1
21	-18.5	0.055	M2-off-mirror
22	-21.5	0.013	M2-on-mirror
23	-23.1	0.018	M2-on-mirror
24	-25.5	0.012	M2-on-mirror
25	-36.7	0.030	M2-off-mirror
26	-61.7	0.094	M1

791 [a] Uncertainty in area is about 9% relative except as noted.

792 [b]less-resolved peaks, uncertainties about 10-30%.

793

794 **Table 7.** Peak positions and areas for 0.25% Co-monticellite.

0.25% Co-monticellite			
Peak	Shift (ppm)	Area (%)[a]	Co-forsterite peak
1	17.6	0.7	3
2	10.5	1.4	6
shoulder	c.a. 2	2.9	
unshifted	0	94	
3	-44.3	0.6	26

795 [a] uncertainty in area is about 10% relative except as noted.

796

797

798

799

800 **Table 8**. M sites within 4 bonds of the silicon site in forsterite (Fujino et al. 1981), and the

801 expected scaling of the areas of associated paramagnetically shifted peaks.

Site	Distance to Si (Å)	Bonds[a]	Equivalent sites	Area scale factor[b]
M1	2.695	2	2	2X
M1	3.253	2	2	2X
M1	4.412	4	2	2X
M1	5.013	4	2	2X
M1	5.334	4	2	2X
M1	6.111	4	2	2X
M1	6.224	4	2	2X
M1	6.245	4	2	2X
M1	6.737	4	2	2X
M2	2.786	2	1	Y
M2	3.250	2	1	Y
M2	3.273	2	1	Y
M2	3.278	2	2	2Y
M2	5.216	4	2	2Y
M2	5.428	4	1	Y
M2	5.513	4	2	2Y
M2	5.560	4	2	2Y
M2	6.024	4	2	2Y
M2	6.071	4	1	Y
M2	6.596	4	2	2Y
M2	6.815	4	2	2Y

802 [a] number of bonds separating M and Si sites, e.g. 4 bonds for M1-O-M2-O-Si.

803 [b] factor by which peak area will be scaled for M1 occupancy of X% and M2 occupancy of Y%.

804

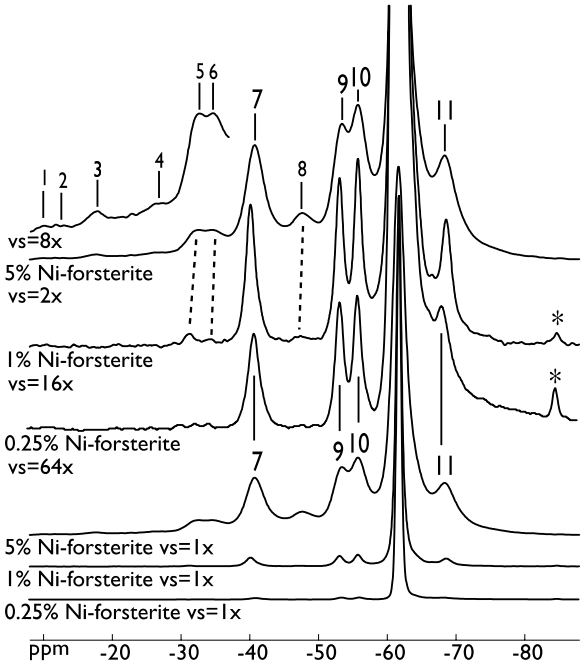

Figure 1. ^{29}Si MAS NMR spectra at 9.4 T (5% and 0.25%) or 14.1 T (1%), 0.05 s pulse delay, of forsterite with three different Ni concentrations, with spinning speeds 15 kHz (5% and 0.25%) and 20 kHz (1%). The lower three spectra are repeated above with their vertical scales enlarged as indicated. Dashed lines are drawn between corresponding double neighbor paramagnetically shifted peaks for samples with different Ni concentrations. * marks unknown impurity phase. Here and in all other figures except Figure 7, all spinning sidebands are well outside of the frequency range shown.

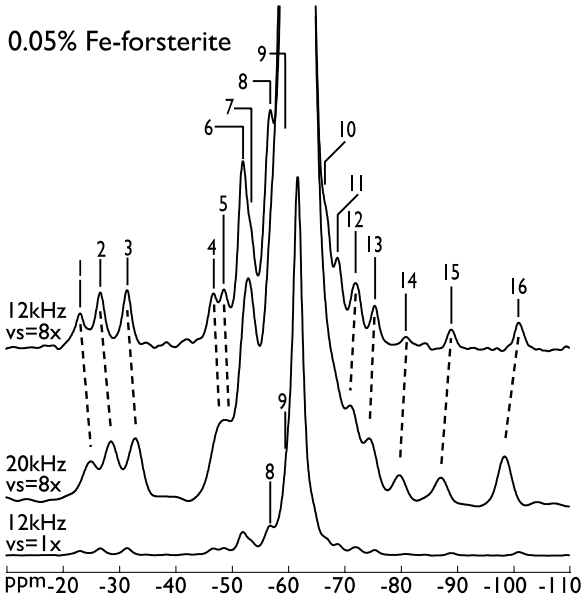

814

815 **Figure 2**. ^{29}Si MAS NMR spectra (14.1 T, 0.05 s pulse delay) of Fe-forsterite at two spinning

816 speeds as shown, illustrating effects of air frictional heating on positions of paramagnetically

817 shifted peaks.

818

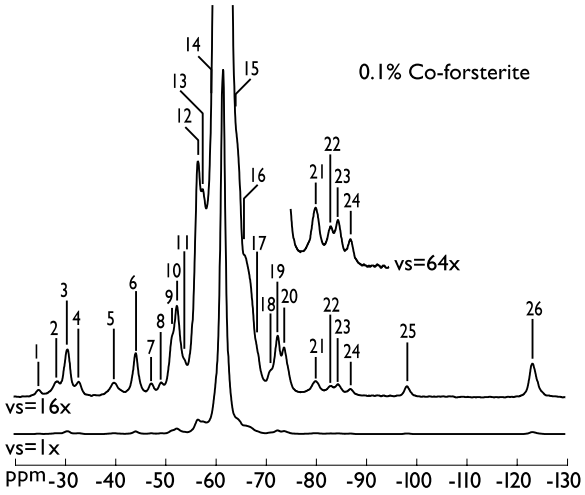

Figure 3. ^{29}Si MAS NMR spectrum (14.1 T, 0.05 s pulse delay) of ^{29}Si enriched forsterite with 0.1% Co at 20 kHz spinning speed.

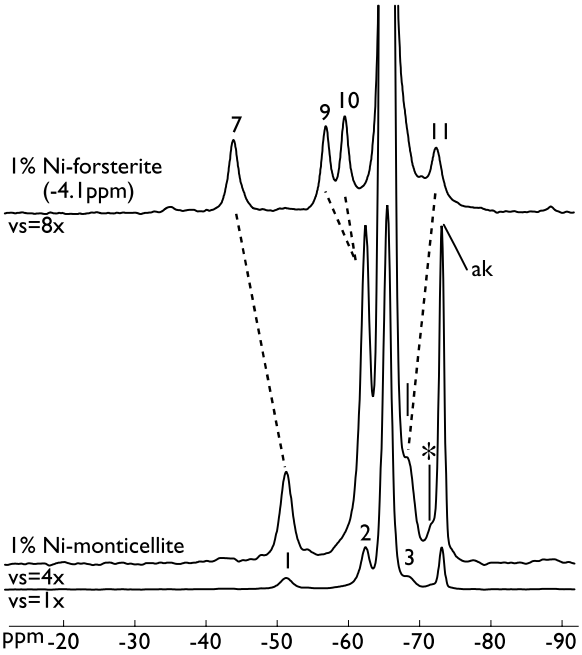

Figure 4. ^{29}Si MAS NMR spectra (9.4 T, 0.05 s pulse delay) of 1% Ni-monticellite and 1% Ni-forsterite both at 15 kHz spinning speed. In the former, the akermanite impurity is labeled with "ak" and an unknown impurity phase with an asterisk. The Ni-forsterite spectrum is shifted -4.1 ppm to align with the unshifted peak of the Ni-monticellite. Dashed lines are drawn between corresponding peaks.

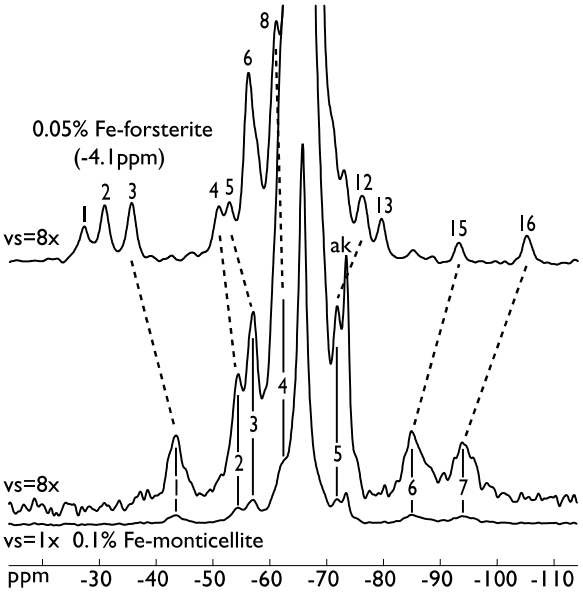

Figure 5. ^{29}Si MAS NMR spectra (14.1 T, 0.05 s pulse delay) of Fe-monticellite and Fe-forsterite at spinning speeds of 20 kHz. In the Fe-monticellite, the akermanite impurity is labeled as "ak". The Fe-forsterite spectrum is shifted -4.1 ppm to align with the unshifted peak of the Fe-monticellite peak. Dashed lines are drawn between corresponding peaks.

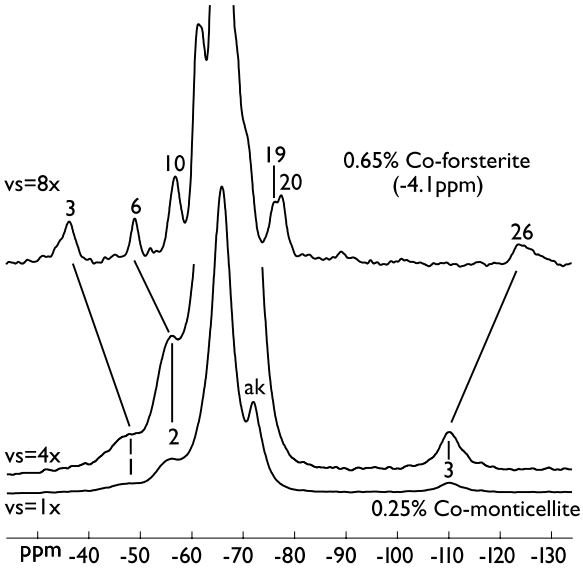

838

839 **Figure 6**. ^{29}Si MAS NMR spectra (14.1 T, 0.05 s pulse delay, 20 kHz spinning speed) of Co-

840 monticellite and Co-forsterite. The akermanite impurity phase is labeled as "ak". The Co-

841 forsterite spectrum is shifted -4.1 ppm to align with the unshifted Co-monticellite peak. Dashed

842 lines mark corresponding peaks.

843

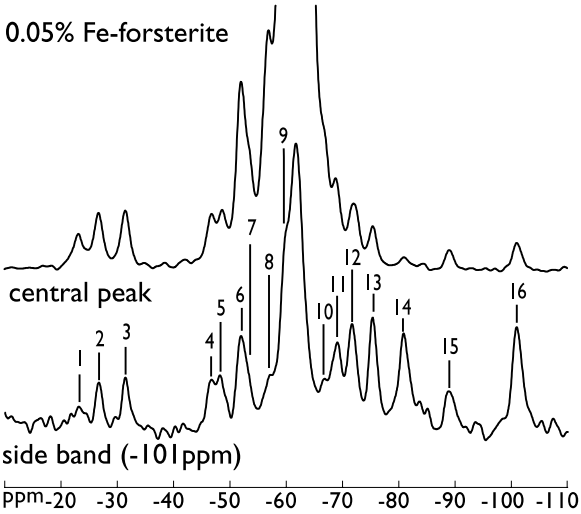

844

845 **Figure 7.** ^{29}Si MAS NMR spectrum of 0.05% Fe-forsterite (as in Fig. 1), comparing the central

846 band of peaks to the first group of spinning side bands to higher frequency, shifted in frequency

847 by -101 ppm. Note the greatly reduced relative intensity of the unshifted resonance in the

848 latter, allowing improved resolution of at least one close-in shifted peak (#9).

849

850

851

852

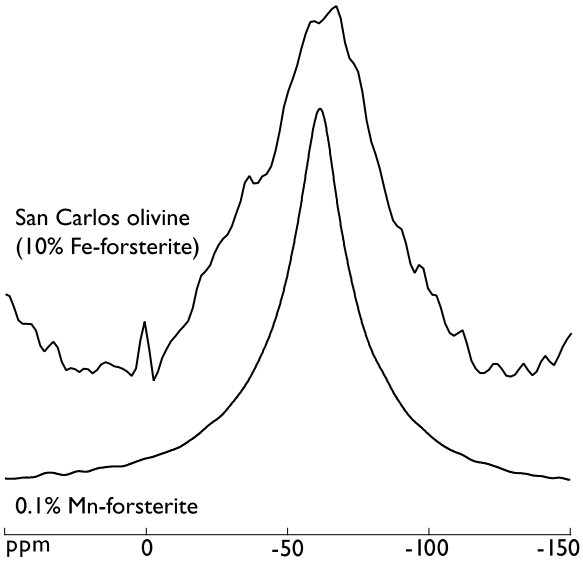

Figure 8. ^{29}Si MAS NMR spectrum (14.1 T, 0.05 s pulse delay) of Mn-forsterite, showing severe line broadening effects of Mn^{2+}. A spin-echo MAS spectrum of San Carlos olivine (9.4 T, 10 kHz spinning speed) is shown to illustrate broadening caused by a much higher Fe^{2+} content. In the latter, the spike at 0 ppm is an artifact, and the inner edges of the first spinning sidebands can be seen in the baseline.

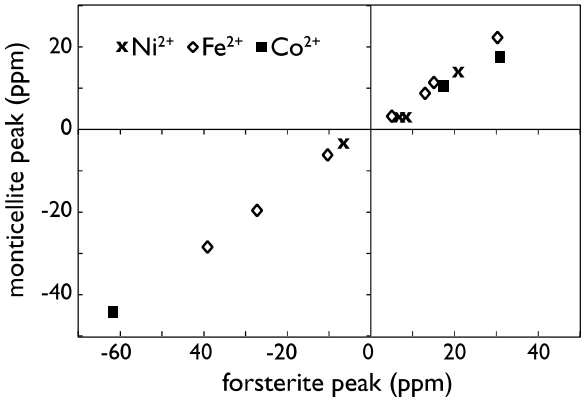

Figure 9. A plot of paramagnetic shifts, relative to the central resonance, for peaks in transition-metal containing forsterite and the corresponding ones in monticellite. Data shown are from spectra collected at 14.1 T and 20 kHz spinning speed.

866

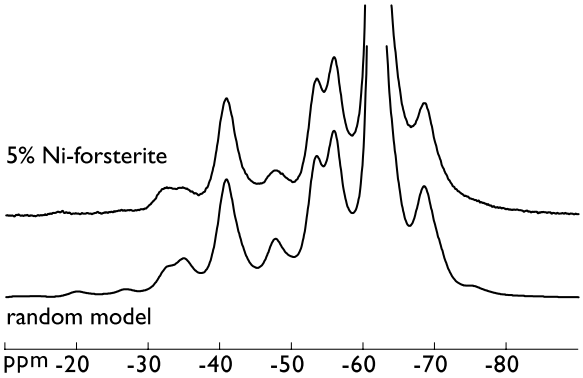

867

868 **Figure 10.** Observed ^{29}Si MAS NMR spectrum of 5% Ni-forsterite (as in Fig. 1), compared with
869 model that assumes random distribution of Ni^{2+} on M1 sites only.